A&A 601, A6 (2017)
DOI: 10.1051/0004-6361/201628762

Astronomy & Astrophysics

Polarimetry of transiting planets: Differences between plane-parallel and spherical host star atmosphere models

N. M. Kostogryz[1], T. M. Yakobchuk[1], S. V. Berdyugina[1], and I. Milic[2,3]

[1] Kiepenheuer-Institut für Sonnenphysik (KIS), Schöneckstrasse 6, 79104 Freiburg, Germany
e-mail: [kostogryz;sveta]@leibniz-kis.de
[2] Max-Planck-Institut für Sonnensystemforschung (MPS), Justus-von-Liebig-Weg 3, 37077 Göttingen, Germany
[3] Astronomical Observatory Belgrade, Volgina 7, 11060 Belgrade, Serbie

Received 21 April 2016 / Accepted 27 February 2017

ABSTRACT

Context. To properly interpret photometric and polarimetric observations of exoplanetary transits, accurate calculations of center-to-limb variations of intensity and linear polarization of the host star are needed. These variations, in turn, depend on the choice of geometry of stellar atmosphere.
Aims. We want to understand the dependence of the flux and the polarization curves during a transit on the choice of the applied approximation for the stellar atmosphere: spherical and plane-parallel. We examine whether simpler plane-parallel models of stellar atmospheres are good enough to interpret the flux and the polarization light curves during planetary transits, or whether more complicated spherical models should be used.
Methods. Linear polarization during a transit appears because a planet eclipses a stellar disk and thus breaks left-right symmetry. We calculate the flux and the polarization variations during a transit with given center-to-limb variations of intensity and polarization.
Results. We calculate the flux and the polarization variations during transit for a sample of 405 extrasolar systems. Most of them show higher transit polarization for the spherical stellar atmosphere. Our calculations reveal a group of exoplanetary systems that demonstrates lower maximum polarization during the transits with spherical model atmospheres of host stars with effective temperatures of $T_{\rm eff}$ = 4400−5400 K and surface gravity of $\log g$ = 4.45−4.65 than that obtained with plane-parallel atmospheres. Moreover, we have found two trends of the transit polarization. The first trend is a decrease in the polarization calculated with spherical model atmosphere of host stars with effective temperatures $T_{\rm eff}$ = 3500−5100 K, and the second shows an increase in the polarization for host stars with $T_{\rm eff}$ = 5100−7000 K. These trends can be explained by the relative variation of temperature and pressure dependences in the plane-parallel and spherical model atmospheres.
Conclusions. For most cases of known transiting systems the plane-parallel approximation of stellar model atmospheres may be safely used for calculation of the flux and the polarization curves because the difference between two models is tiny. However, there are some examples where the spherical model atmospheres are necessary to get proper results, such as the systems with grazing transits, with Earth-size planets, or for the hot host stars with effective temperatures higher than 6000 K.

Key words. polarization – methods: numerical – planetary systems

1. Introduction

Since the first exoplanet orbiting a solar-type star was discovered (Mayor & Queloz 1995) more than 2500 exoplanets have been discovered (see Extrasolar Planets Encyclopaedia[1]). The transit method for their detection and characterization became particularly interesting after the *Kepler* mission started operating (Borucki et al. 2010; Koch et al. 2010). Polarimetry is a complementary technique that provides additional information about planetary atmospheres, about the parameters of their orbits, and about the host stars themselves. With the development of polarimeters with high sensitivity, i.e., PlanetPol (Hough et al. 2006), DIPOL-2 (Piirola et al. 2014), POLISH (Wiktorowicz & Matthews 2008), and HIPPI (Bailey et al. 2015), a polarimetric investigation of exoplanets became feasible (e.g. Berdyugina et al. 2008, 2011; Lucas et al. 2009; Wiktorowicz et al. 2015; Bott et al. 2016).

In this paper, we investigate an interesting polarimetric effect that arises during a planetary transit. By breaking the symmetry of the intensity distribution over the stellar disk, a transiting planet causes the light, emitted by the partially eclipsed star, to be linearly polarized. This effect was first observed in the eclipsing binary Algol by Kemp et al. (1983). Later, it was theoretically calculated for the case of transiting extrasolar planets by Carciofi & Magalhães (2005) and Kostogryz et al. (2011, 2015). The first attempt to detect the polarimetric signal of an exoplanetary system, HD 80606b, during a transit was not successful (Wiktorowicz & Laughlin 2014). This target has a bright host star with a long transit ingress, which is good for observations. However, it has a small planet-to-star radius ratio and low intrinsic stellar polarization leading to a very small polarization signal during transit. Using the observationally inferred parameters of HD 80606b, our theoretical prediction for its maximum polarization during the transit is below the current polarimetric sensitivity limit of 3×10^{-6} (Kostogryz et al. 2015).

In addition to orbital and physical parameters of a system, the stellar limb darkening is needed to model the flux curve during a transit. The calculation of the polarimetric curve requires additional information about the stellar limb polarization. The main input for calculation of center-to-limb variation of the

[1] http://exoplanet.eu

intensity (CLVI) and the polarization (CLVP) is a stellar model atmosphere, that can be presented in various approximations, i.e. a plane-parallel model (PPM) or a spherical model (SphM). We recently computed the CLVI and CLVP in the continuum assuming a PPM (Kostogryz & Berdyugina 2015) and a SphM (Kostogryz et al. 2016) stellar atmospheres at different effective temperatures and surface gravity.

Kostogryz et al. (2015) calculated the polarization during the transits of 88 known extrasolar planets assuming a PPM stellar atmosphere, and selected the most promising targets for observations. In the present paper, we calculate the polarimetric curves during transits for 405 known exoplanets with SphM and PPM stellar atmospheres using the CLVI and CLVP calculated for these two geometries from Kostogryz et al. (2016) and Kostogryz & Berdyugina (2015), respectively. The SphM geometry is closer to reality; however, the PPM is computationally simpler. Therefore, in order to understand whether simpler PPM stellar model atmospheres may be used for interpretation of transit light curves, we calculate the differences in predicted polarization during transit that can arise from these stellar atmosphere geometries, and compare our results obtained with PPM and SphM. In Sect. 2, we briefly describe the method for the calculation of flux and polarization during transits and discuss some modifications that are needed to take the SphM geometry of a stellar atmosphere into account. Section 3 contains the results of our computations and comparisons with PPM stellar atmospheres. In Sect. 4, we discuss some situations when the polarized signal of exoplanetary system calculated with PPM significantly deviates from the SphM calculations. Finally, in Sect. 5 we summarize the results and draw conclusions.

2. Calculation of the transit polarization

The method for calculating the polarization during a transit is described in Kostogryz et al. (2015). Here we recall the main idea of this study.

When a planet transits its host star, it blocks part of the stellar radiation, which travels from the star to the observer, which decreases the stellar flux. For a given set of parameters describing the configuration of the planetary system, we calculate the residual stellar flux and normalized Stokes parameters $q = Q/I$ and $u = U/I$, as well as polarization degree describing linear polarization.

To calculate the flux and the Stokes parameters during a transit, the center-to-limb variations of the intensity and the linear polarization should be known. We use the CLVI and the CLVP calculated for PPM (Kostogryz & Berdyugina 2015) and SphM (Kostogryz et al. 2016) geometries of stellar atmospheres to study the variations in resulting flux and polarization during planetary transits.

The center-to-limb variation of the intensity and the polarization calculated for a PPM can be directly used in our method, while it cannot be used for a SphM. As described by Kostogryz et al. (2016), the calculated CLVI and CLVP for a SphM atmosphere provide information on the limb position of the stellar disk, i.e., the exact value of the stellar radius. The limb of a star is chosen at the location on the stellar disk, which is characterized by $\mu = \mu_{\rm limb}$ ($\mu = \cos\theta$, where θ is the angle between the direction normal to the surface and the line of sight, and $\mu_{\rm limb}$ corresponds to the value of μ where the largest gradient of the center-to-limb variation of intensity is observed). For different stellar atmospheres the position of the limb is related to different μ. This brings up an interesting question of what should be considered to be the radius of the stellar disk. To use the CLVI and the CLVP calculated for SphM atmospheres, all curves need to be calculated with respect to the limb position – μ should be equal to 0 at the limb (Fig. 5, solid line) as it is for PPM atmospheres (Fig. 5, dashed line) – or the radius of a star needs to be expanded in order to use the whole calculated curves. Using the curves that are calculated with respect to a limb position, all information about the intensity and the polarization outside the limb is therefore lost. The intensity outside the limb is very small, and expanding the stellar radius does not influence the transit depth very much. However, the polarization outside the limb is very high and can contribute slightly to the resulting polarization during transit, especially for a grazing transit. From now on, we appropriately scale (i.e., increase) the radius of the star to take the whole CLVI and CLVP curves into account.

For the stars in our study we note that we use the same effective temperatures for both the PPM (Hauschildt et al. 1999) and the SphM (Husser et al. 2013), although their values were determined in the literature by fitting stellar spectra using PPMs only. We admit that if the same procedure is applied to SphMs, it is possible that somewhat different effective temperatures could be obtained. Checking the possible difference is, however, beyond the scope of this paper. If in the future effective temperatures are changed for the stars when analyzed with SphMs, we refer the reader to the paper by Kostogryz et al. (2016).

3. Results

We compare the fluxes, the Stokes parameters (q, and u), and the polarization degrees computed for a sample of known exoplanets assuming SphM and PPM atmospheres of the host stars. Below, we first briefly discuss the results for a sample of 405 known extrasolar planets, and after that we analyze two individual cases in detail. All required physical and orbital parameters of the planetary systems are taken from the Exoplanets Orbit Database[2] (EOD, Han et al. 2014) and the Extrasolar Planets Encyclopaedia[1] (EPE).

3.1. Transit exoplanets

To date, more than 2500 transiting planetary systems have been confirmed. We have prepared a sample of all transiting exoplanets with known inclination angles resulting in the selection of 405 exoplanets from the EPE and the EOD. In Fig. 1 we plot the maximum polarization degree assuming SphM atmospheres of the host stars versus the surface gravity for different effective temperatures and planet-to-star radius ratios based on our sample of transiting exoplanets. We note that the maximum polarization occurs around ingress and egress of transiting planet. Depending on the inclination angles, ingress and egress can occupy a relatively small fraction of transit ($i = 90$ deg), a larger fraction ($i < 90$ deg), or even the whole transit curve for nearly grazing transit. We label the targets with the highest level of transit polarization in the figure. The maximum polarization values are calculated at 200 points covering the transit at 4500 Å. We note that the maximum polarization degree during transit for all exoplanetary sytems is almost two times higher at 4000 Å than at 4500 Å.

To show how much the geometry of a stellar atmosphere affects the transit polarization, in Fig. 2 we present the ratio of the maximum transit polarization calculated with SphM to the value calculated with PPM atmospheres depending on the effective temperature and surface gravity of the host stars. Most of

[2] http://exoplanets.org

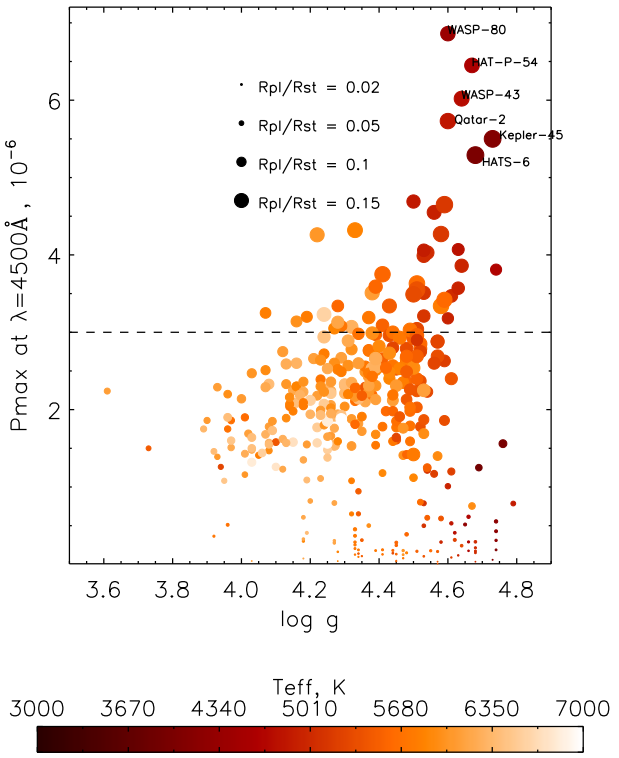

Fig. 1. Maximum transit polarization at 4500 Å for a sample of 405 exoplanets for a SphM atmosphere of the host stars. The dashed line depicts the lower limit of the achievable polarization sensitivity, $P = 3 \times 10^{-6}$. We note that the sensitivity strongly depends on photon flux. The color scale refers to the effective temperature of a particular star. The planet-to-star radius ratios are indicated by the size of the circles.

the known extrasolar planetary systems are predicted to show higher polarization degrees for the SphM stellar atmosphere. However, there are exoplanetary systems with a ratio smaller than 1.0, i.e., the maximum polarization during transit is higher with PPM. For example, in Fig. 2, panel a, there is a compact group of exoplanetary systems within the range of surface gravity $\log g \approx 4.45{-}4.65$ where the PPM atmosphere overestimates polarization of the host star. The range of effective temperatures of this group of host stars can be obtained from panel b, and it is between ≈4400−5400 K. So, combining panels a and b in Fig. 2, it is possible to identify stars where the maximum polarization degree during transits is larger with the PPM atmosphere. This group has effective temperatures of $T_{\rm eff} \approx 4400{-}5400$ K and surface gravity of $\log g \approx 4.45{-}4.65$.

The main reason for the deviations in transit polarization is a difference in model temperature-pressure dependences and, therefore, in calculated absorption and scattering opacities of PPM and SphM stellar atmospheres. For the same effective temperature and surface gravity two model atmospheres, PPM and SphM, are not identical. In Fig. 3 we present the stratifications of temperature (a) and normalized opacity (b), as well as center-to-limb variation of intensity I/I_0 (c) and polarization q (d) for the PPM and SphM atmosphere models with effective temperature of $T_{\rm eff} = 5000$ K and $\log g = 4.5$. This particular model contributes to the group of exoplanetary systems that shows a lower value of maximum transit polarization for SphM than for PPM. The I/I_0 is the normalized intensity over the stellar disk relative to the disk center. Figure 3, panel a), shows that PPM has higher temperature in the very top ($\tau \approx 1 \times 10^{-6}$) and in the deep layers ($\tau > \approx 2{-}3$) of the atmosphere than SphM does. Naturally this variation of temperature leads to variation in I/I_0 and q. In particular, the temperature increase in the lower layers leads to intensity increase in the center of the stellar disk, while the temperature increase in the upper layers leads to intensity increase close to the limb. If the intensity close to the center of the disk increases and the intensity at other disk positions does not change, we observe the stronger limb darkening effect. Therefore, the I/I_0 is lower for PPM than for SphM.

We now consider how the polarization changes in the stellar atmosphere. Light scattering in a stellar atmosphere produces polarized radiation of the star. When the layer where scattering exceeds absorption lies deeper in the model atmosphere, we can expect higher polarization (for more details, see Kostogryz & Berdyugina 2015; Kostogryz et al. 2016). In Fig. 3b normalized opacities for PPM and SphM are presented. The level in the atmosphere where the absorption and scattering opacities are equal is slightly deeper in the SphM atmosphere than in the PPM one. Therefore, we expect slightly higher polarization in CLVP calculated with SphM. However, we obtain the ratio of normalized Stokes parameter q slightly lower for SphM atmosphere (Fig. 3d) because the difference in I/I_0 is larger than the difference in Stokes Q. Therefore, the ratio of Q/I is slightly larger for PPM than for SphM atmosphere.

To understand the increase in maximum transit polarization for SphM starting from $T_{\rm eff} = 5400$ K (see Fig. 2), we make the same analysis for atmospheric models with $T_{\rm eff} = 6500$ K and $\log g = 4.5$ (Figs. 3e-h). In this case, the temperature distributions for the two models, PPM and SphM, almost coincide, except of very deep layers in the atmosphere, where the SphM atmosphere is hotter (Fig. 3e). The hotter deep layers of the SphM atmosphere cause a decrease in I/I_0 (Fig. 3g) and an increase in q (Fig. 3h). The scattering opacity exceeds the absorption slightly deeper in the SphM atmosphere (Fig. 3f), which also leads to an increase in q (Fig. 3h). Since the calculation of linear polarization for transiting exoplanetary systems requires the center-to-limb variation in both intensity and polarization, a combination of these variations on a stellar disk calculated with different models, SphM and PPM, causes the variation in maximum polarization during planetary transit.

Figure 2b shows two trends of maximum transit polarization ratio calculated for SphM and PPM atmospheres with an increase in effective temperatures of host stars. First, the ratio decreases for the range of effective temperatures $T_{\rm eff} = 3500{-}5100$ K and then it increases for higher temperatures. These trends can be explained by the variations in temperature stratifications between the two models, SphM and PPM. In Fig. 4 averaged temperature differences between SphM and PPM for the ranges of optical depths, $\tau_1 \leq 1 \times 10^{-4}$ (upper panel) and $\tau_2 \geq 2$ (lower panel) are shown. The positive values indicate that the SphM atmospheres are hotter and the negative values that they are cooler for the same values of effective temperature and surface gravity. The temperature difference in the lower atmosphere (Fig. 4, lower panel) correlates with the behavior of the maximum transit polarization (Fig. 2b). Namely, it decreases until $T_{\rm eff} = 5100$ K and then increases. The averaged differences $T^1_{sp}{-}T^1_{pp}$ (Fig. 4, upper panel) show a similar trend and affects the opacity at the top of the atmosphere. We note that two PHOENIX spherical models with $T_{\rm eff} = 4200$ K and 6000 K with $\log g = 4.0$ (blue squares) are outliers. We omit these models in our calculations, and interpolate between the neighboring calculations to get the polarization for the host stars. We recommend avoiding calculations for these two models when using the CLVP from Kostogryz et al. (2016), where the Phoenix spherical models were used.

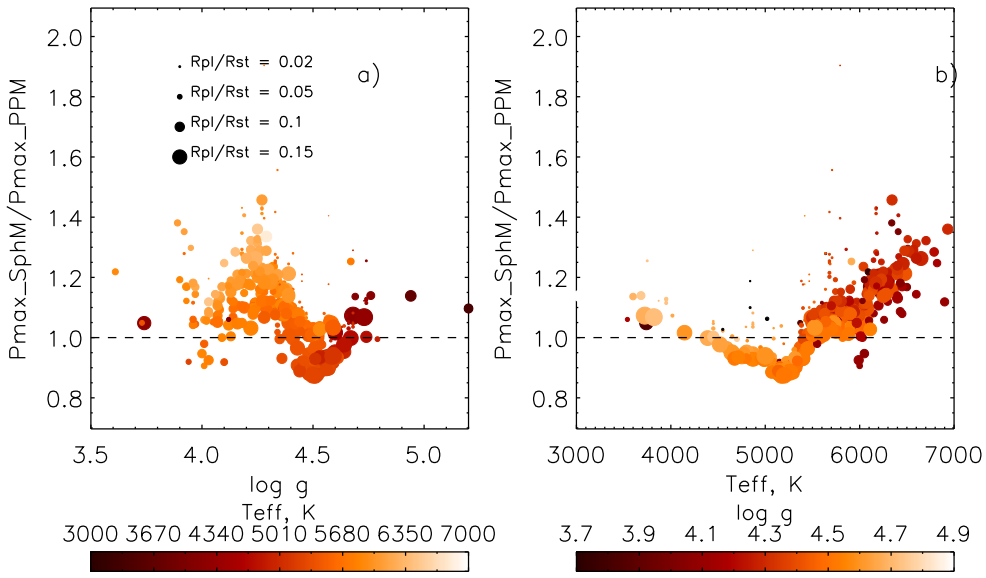

Fig. 2. Ratio of maximum polarization of exoplanetary system during transit calculated with SphM to that calculated with PPM stellar atmospheres depending on gravity **a)** and temperature **b)** for all considered host stars at 4500 Å. The color scale in **a)** describes the temperature of the host stars and in **b)** presents their surface gravity. The size of the circles indicates the planet-to-star radius ratio. The dashed line indicates the equal value for maximum transit polarization obtained with SphM and PPM stellar atmospheres.

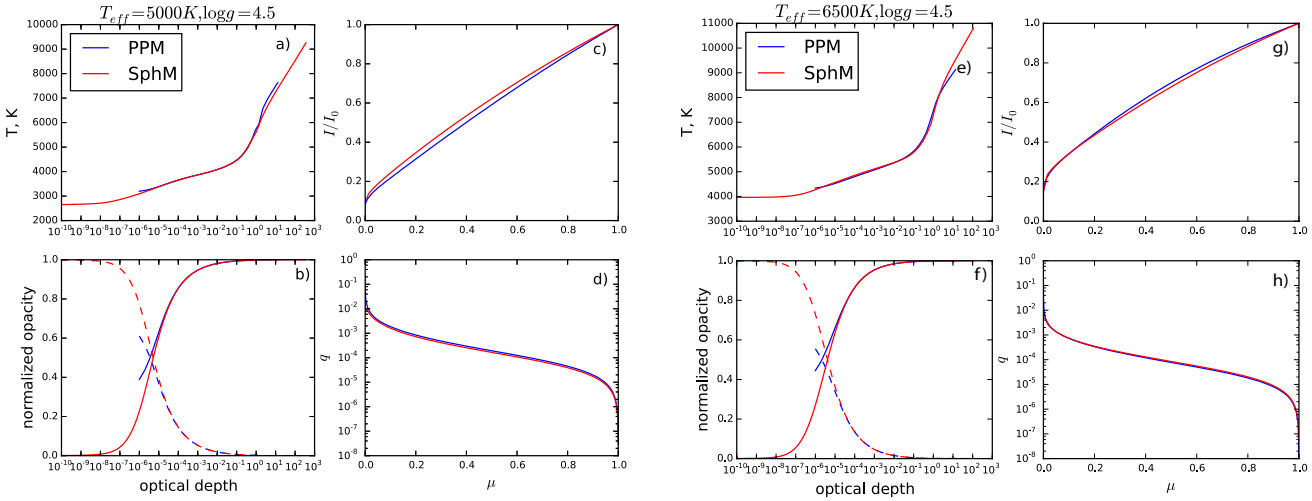

Fig. 3. **a)** Temperature stratifications for two different PPM (blue line) and SphM (red line) stellar models with effective temperature of $T_{\rm eff}$ = 5000 K and $\log g = 4.5$. **b)** Stratification of normalized absorption (solid line) and scattering (dashed line) opacities for PPM (blue) and SphM (red) of the stellar atmospheres with $T_{\rm eff}$ = 5000 K. **c)** Center-to-limb variation of intensity for PPM (blue line) and SphM (red line). **d)** Center-to-limb variation of polarization for PPM (blue line) and SphM (red line). The panels **e)–h)** show the same values as in **a)–d)**, but for stellar models with $T_{\rm eff}$ = 6500 K and the same value of surface gravity, respectively.

There are several other outliers from the trends. This can happen if there are other parameters that also influence the results. For example, if the planet-to-star radius ratio is large, the planet diminishes high values of local polarization on the stellar limb during ingress or egress because a larger part of the star is eclipsed (see the small circles in Fig. 2). For Earth-size planets orbiting stars with $T_{\rm eff} \geq 5400$ K, the SphM atmospheres provide higher signals. Therefore, we recommend using the CLVI and CLVP calculated with the SphM atmosphere to interprete the transit light curves. The inclination angle of the planetary orbit also affects the value of the maximum polarization during transit, especially grazing transit (see Sect. 3.3).

We would like to note that detecting such a level of polarized signal is extremely challenging. In order to reach the sensitivity limit of 3×10^{-6} (3σ), it is necessary to integrate over a long time to get enough photons. For example, for one of the brightest transit exoplanetary systems (HD 189733) with an apparent magnitude in B of 8.58, the photon noise error obtained with DiPOL-2 (Piirola et al. 2014) at a 4 m telescope and 10 min of integration time is about 1.8×10^{-5} (V. Piirola, priv. comm.). Here, we want to emphasize that the maximum polarization of 3.99×10^{-6} for HD 189733 (see Fig. 6) is calculated assuming 200 points per transit which implies an exposure time of about 40 s per measurement. For more realistic measurements with longer exposure times, we averaged the Stokes parameters assuming that we can only get 10 measurements per transit for each q and u. Then, the averaged maximum polarization for HD 189733 is equal to 3.58×10^{-6} at 4500 Å. To confidently detect the signal of the averaged maximum polarization, the noise level should be at least 1.2×10^{-6}. To achieve 1.2×10^{-6}, it is

Table 1. Integration times and number of transits on the different telescopes with the DiPOL-2.

Name	m_B	$P_{\max}^{\text{aver}}, 10^{-6}$	Δt, hours			Number of transits		
			4 m	8 m	39 m	4 m	8 m	39 m
HD 189733b	8.58	3.58	40	20	4	182	90	18
HD 209458b	8.21	2.27	50	25	5	167	84	17
WASP-33b	8.63	1.41	279	139	28	2487	1244	248
KELT-7b	8.97	1.35	569	259	57	3889	1945	389

Notes. m_B is the stellar brightness magnitude in B band and $P_{\max}^{\text{aver}}$ is the averaged values of maximum polarization during the transit. The average number of measurements per transit is 10, i.e., exposure time is assumed to be 1/10 of transit time. $P_{\max}^{\text{aver}}$ is given for this exposure time.

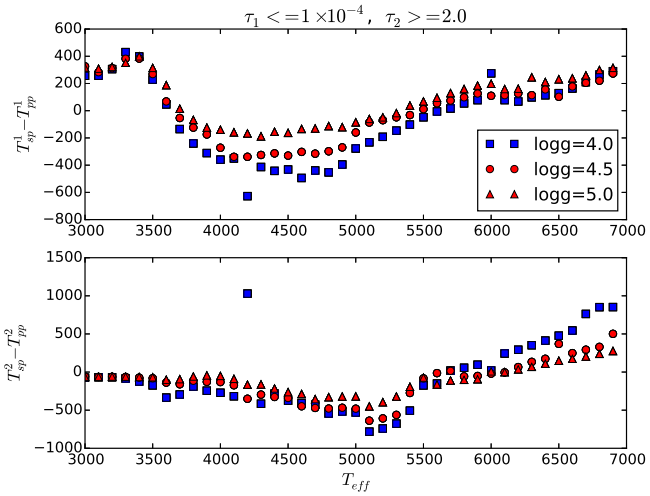

Fig. 4. Temperature difference between PHOENIX SphM and PPM averaged for an optical depth range of $1\times10^{-6} \le \tau \le 1\times10^{-4}$ (*upper panel*) and $\tau \ge 2$ (*lower panel*) for all used models.

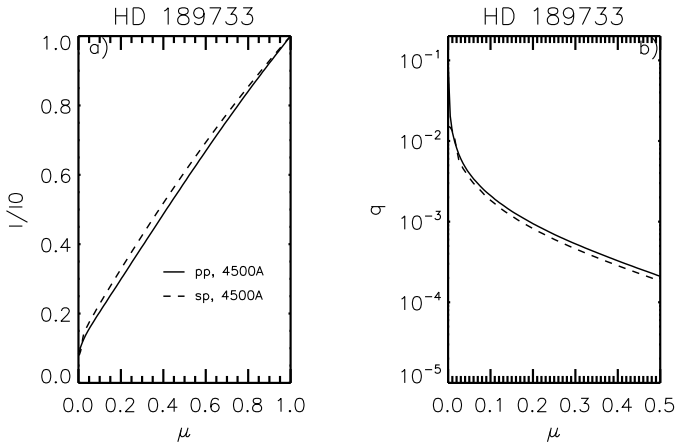

Fig. 5. Center-to-limb variations of the intensity **a)** and the scattering polarization in continuum **b)** for HD 189733 at 4500 Å. The dashed line describes the results of our calculations for the SphM atmosphere. Our calculations for the PPM atmosphere are presented as a solid line.

necessary to integrate almost 40 h per exposure bin at a 4 m telescope. On the other hand, with a larger telescope the integration time decreases, e.g., with an 8 m telescope it is almost 20 h and with a 39 m telescope it becomes 4 h. The values of integration time per exposure bin for the brightest exoplanetary systems for different telescopes are presented in Table 1. To detect a variation of polarization during a transit, it is necessary to integrate the polarized signal over many transits for the same part of transit curve. To diminish the effect of stellar activity on the polarized signal, at least three measurements are needed: before, the transit, at maximum, and after the transit. The number of transits needed to detect the polarized signal of the selected targets with DiPOL-2 mounted on different telescopes are shown in Table 1.

Since the local linear polarization on the stellar disk is greater for cooler stars within the considered surface gravity values (Kostogryz & Berdyugina 2015; Kostogryz et al. 2016), the maximum polarization degree during transits is expected to be higher for cooler stars. However, for dimmer exoplanetary systems the integration time increases. Nevertheless, the polarized signal that arises during a planetary transit provides unique information that is very useful for our understanding of planetary systems. With the forthcoming space missions TESS (Ricker 2015) and PLATO (Rauer et al. 2014), which will detect transiting planets around bright stars, we may have a possibility to measure polarized signals of exoplanetary systems during transits in the near future.

3.2. HD 189733b

HD 189733b was discovered by Bouchy et al. (2005); its high brightness (m_v = 7.67), large planet-to-star radius ratio ($R_p/R_s \approx 0.15$), and short orbital period ($P \approx 2.2$ days) make it one of the best studied transiting exoplanets. In addition to the set of parameters from EOD, for HD 189733b, we use the longitude of ascending node $\Omega = 195$ deg and inclination angle $i = 94.49$ deg derived from polarimetric measurements (Berdyugina et al. 2008, 2011).

Here we model the flux and polarization variations of this system during transit for PPM and SphM atmosphere of the host star. In Fig. 5 a comparison of the I/I_0 and q between the SphM and the PPM atmospheres at 4500 Å is presented. Figure 5 shows that when the PPM approximation is used to describe the stellar atmosphere of HD 189733, the limb darkening is underestimated, while the limb polarization is overestimated compared to the calculations with the SphM atmosphere.

Using the calculated CLVI and CLVP, we compute the variation in the flux, Stokes q and u, and the polarization degree during transit at 4500 Å (Fig. 6) in order to understand how much these effects, the underestimation of the intensity, and overestimation of the polarization, affect the light curves. The relative flux almost does not change, and the only place where a tiny difference appears is the duration of the transit. This difference may be misinterpreted to provide a slightly incorrect inclination angle. In the polarization curves (right panel in Fig. 6) the difference is more prominent, but still very small.

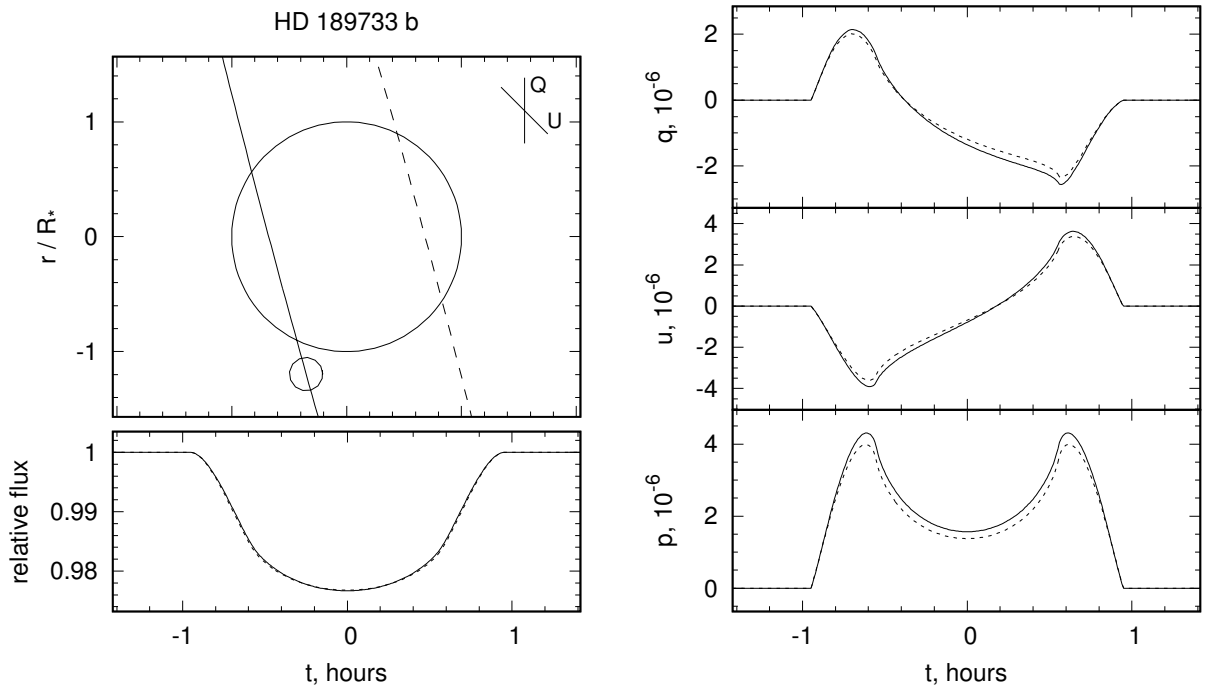

Fig. 6. Configuration of HD 189733 and the modeled variations of the flux and polarization (q, u, and p) at 4500 Å. The planet is orbiting from the bottom to the top in front of the star. Solid and dash-dotted lines represent the calculations for the PPM and SphM atmospheres for the host star, respectively. The dashed line in the *top left panel* defines the planetary orbit behind the star.

With the stellar physical parameters of HD 189733, $T_{\rm eff}$ = 5040 K, and $\log g$ = 4.587, the center-to-limb variation of the polarization is lower for SphM atmosphere resulting in lower polarization during the transit.

We conclude that the variation between the two models is negligible in intensity light curve and tiny (about 8%) in polarized curves. Therefore, for this particular system, the simpler PPM stellar atmosphere can be used to characterize the transit light curves.

3.3. Grazing exoplanet Kepler-447b

The extrasolar planet Kepler-447b was detected by the *Kepler* mission and confirmed by Lillo-Box et al. (2015) as a hot Jupiter with an extremely grazing transit. It orbits a G8 main sequence star that is slightly larger than our Sun ($R_\star/R_\odot$ = 1.05) on a comparatively small separation; the ratio of semi-major axis to stellar radius ($a/R_\star$) is ≈20.4 (Lillo-Box et al. 2015). As there are no polarimetric measurements of Kepler-447b and therefore no information about the longitude of ascending node, we assume Ω = 90 deg.

Because of the smaller intensity at the stellar limb due to the limb darkening effect, photometry faces the problem of how to correctly describe grazing transits. Polarimetry is very sensitive to grazing transits as scattering polarization of a star is highest at the limb. An extreme limb can be correctly described when a SphM stellar atmosphere is considered. Figure 7 presents the I/I_0 and q for Kepler-447 considering SphM and PPM stellar atmospheres. It shows that the polarizations for the PPM and SphM approximations agree except for the very limb where an increase in polarization for the SphM is observed.

Figure 8 describes the flux and polarization variations during the transit of Kepler-447b. Assuming the SphM for the star, we obtained a slightly deeper transit curve, as occurred with the

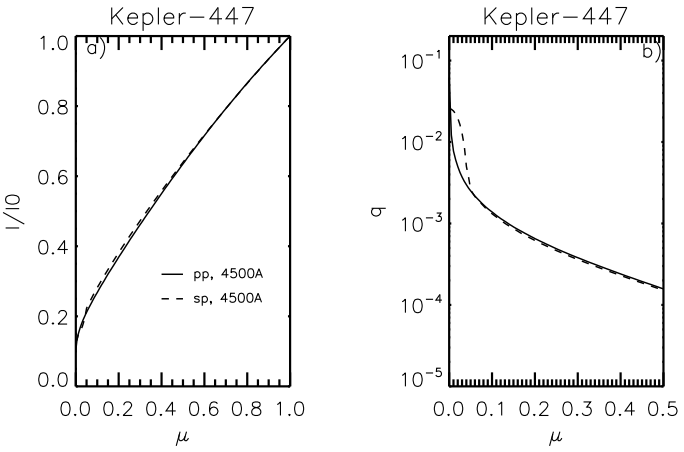

Fig. 7. As in Fig. 5, but for Kepler-447.

PPM for the same planet-to-star radius ratio. The planet-to-star radius ratio is derived from the transit depth of a light curve. Since the SphM atmosphere provides a deeper transit curve (Fig. 8), it is possible to misinterpret such depth and obtain a higher value of planetary radius using CLVI and CLVP calculated with the PPM atmosphere. The CLVP is larger at the limb for the SphM atmosphere of Kepler-447 ($T_{\rm eff}$ = 5493 K and $\log g$ = 4.4) (Fig. 7b). As the planet crosses the very limb of the star, where the polarization with SphM is higher, the predicted polarization during transit is higher.

Normally, the grazing transit depths have very low values, 10^{-3}–10^{-4} level. Therefore, to analyze the light curves of grazing transit planets, we recommend using the SphM atmospheres in both intensity and polarization light curves to avoid errors in estimation of exoplanetary system parameters.

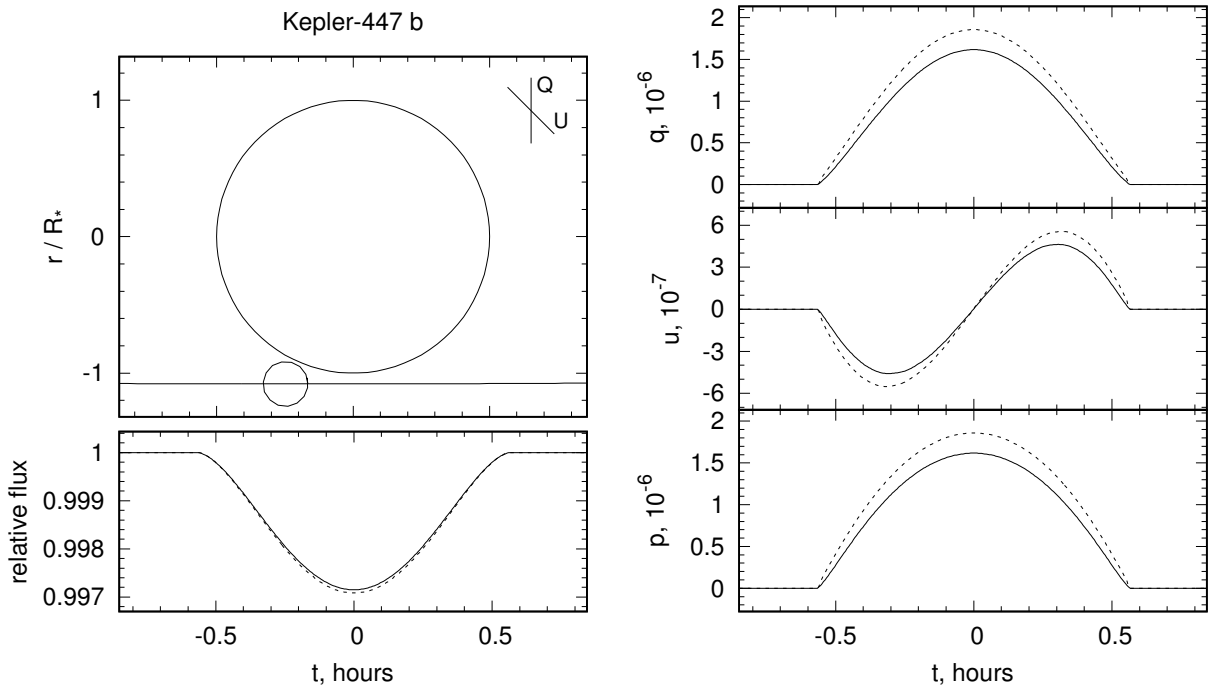

Fig. 8. Same as in Fig. 6, but for the grazing transit exoplanetary system Kepler-447.

4. Discussion

Disk-integrated linear polarization that arises when a planet transits a star strongly depends on the physical and orbital parameters of the system and on the center-to-limb variation of the intensity and polarization of the host star. The exoplanetary community continuously improves the parameters of systems that causes the variation of the values in the EPE and EOD. We take such orbital and physical parameters of exoplanetary system that were established in July 2016. In this paper we compare two different geometries of the stellar atmosphere, PPM and SphM, and demonstrate that predicted polarization during transit depends on this choice. It is obvious that SphM geometry is closer to reality. However, the difference between the two can be small in some cases (e.g. for dwarf host stars), where PPM produces the same results, while offering advantages such as computational simplicity and speed.

The type of model atmosphere adopted for the calculation leads to CLVI and CLVP that differ from our previous calculations. Here, we use PPM and SphM PHOENIX model atmospheres calculated by Hauschildt et al. (1999) and Husser et al. (2013), respectively. Recently, Harrington (2015) calculated linear polarization in the continuum for plane-parallel MARC stellar atmosphere models (Gustafsson et al. 2008) and found it systematically higher (by ≈15% than in Kostogryz & Berdyugina (2015) for the same effective temperature and surface gravity. It was suggested by Harrington (2015) that this difference results from the contribution of spectral lines in his calculations which change the continuum level. Spectral lines are important for ultraviolet wavelengths and cooler stars where "real" continuum is hardly observed. For wavelengths larger than 4000 Å and hotter stars, this is not the case because the line contribution is reduced, and the results of Harrington (2015) have to converge to the continuum case by Kostogryz et al. (2016). Therefore, the difference in our results may be due to other factors where the employed stellar model atmospheres differ. For example, for different semi-analytical solar model atmospheres, the resulting CLVP are different (see, Fig. 5 in Kostogryz & Berdyugina 2015 and Fig. 8 in Kostogryz et al. 2016). This difference in CLVP needs to be clarified because it affects a predicted polarization of the exoplanetary system during transit as well.

Polarimetric observations of exoplanetary transits should be made in broadband filters in order to get more photons on the detector. In the wavelength range of a broadband filter, a large number of spectral lines exist in the stellar spectrum. After including spectral atomic and molecular lines into calculations of limb darkening and limb polarization of stars, an additional variation of calculated CLVI and CLVP in wavelengths can be expected. Therefore, after such modifications, the curves of polarization during transit can look somewhat different. However, the main point of this work, i.e., the difference between plane-parallel and spherical model atmospheres, is likely to stay the same as it only influences geometrical aspects of radiative transfer problem, except for spectral lines that are formed higher in the stellar atmosphere.

5. Summary and conclusions

In this paper, we have calculated the relative fluxes and polarization during the transits of known exoplanets employing the calculated center-to-limb variations of the intensity and the scattering polarization for plane-parallel and spherical stellar atmospheres. Depending on the physical parameters of the host stars, such as effective temperature and surface gravity as well as planet-to-star radius ratios, the polarization that arises during transit can be higher or lower than that obtained with a plane-parallel atmosphere for host stars.

Most of the host stars show higher transit polarization with the center-to-limb variation of the polarization calculated for the spherical atmospheres. One exception is a group of host stars with effective temperatures $T_{\rm eff} \approx 4400-5400$ K and surface gravity $\log g = 4.45-4.65$. We have also found the trends of decreasing transit polarization calculated with spherical models of stellar atmospheres for the range of effective temperatures from

3500 K to 5100 K, and then increasing polarization towards the hotter temperatures. The physics of these trends is explained by the variation in temperature-pressure stratifications resulting in opacity variation for the spherical and plane-parallel models with the same effective temperatures and surface gravity.

For HD 189733 b, the result of our calculations shows a lower expected polarization during transit when we adopt a spherical stellar atmosphere. The relative flux almost does not change. For this system, the simpler plane-parallel model atmosphere can be used.

For the grazing transit system Kepler-447 b, both intensity and polarization are affected by the choice of stellar model atmosphere. The difference between plane-parallel and spherical models of stellar atmospheres leads to tiny difference in transit light curves. However, as the signal of grazing transit is also very small, the tiny difference in stellar models becomes significant. For this system, a spherical model atmosphere is necessary when analyzing grazing transit curves.

We conclude that the relative flux of transit light curves has small differences ($\sim 10^{-4}$) between the two approximations of the stellar atmosphere. For the exoplanetary systems with very small transit signals, relative flux of about 10^{-3}–10^{-4}, the spherical model atmospheres are needed for the accurate analysis of intensity and polarization variations during the planet transits. For other cases, the plane-parallel model atmosphere can be used. The polarization (Stokes q, u, and polarization degree) is more sensitive to these model choices. Calculations of the center-to-limb variation of the polarization with spherical models better describe the polarizaion light curves during planetary transits.

Acknowledgements. This work was supported by the European Research Council Advanced Grant HotMol(ERC-2011-AdG291659). We thank our anonymous referee, Martin Kürster, Oleksii Kuzmychov and Jeff Kuhn for comments and suggestions that improved this paper.

References

Bailey, J., Kedziora-Chudczer, L., Cotton, D. V., et al. 2015, MNRAS, 449, 3064
Berdyugina, S. V., Berdyugin, A. V., Fluri, D. M., & Piirola, V. 2008, ApJ, 673, L83
Berdyugina, S. V., Berdyugin, A. V., Fluri, D. M., & Piirola, V. 2011, ApJ, 728, L6
Borucki, W. J., Koch, D., Basri, G., et al. 2010, Science, 327, 977
Bott, K., Bailey, J., Kedziora-Chudczer, L., et al. 2016, MNRAS, submitted [arXiv:1603.05745]
Bouchy, F., Udry, S., Mayor, M., et al. 2005, A&A, 444, L15
Carciofi, A. C., & Magalhães, A. M. 2005, ApJ, 635, 570
Gustafsson, B., Edvardsson, B., Eriksson, K., et al. 2008, A&A, 486, 951
Han, E., Wang, S. X., Wright, J. T., et al. 2014, PASP, 126, 827
Harrington, J. P. 2015, in IAU Symp., 305, 395
Hauschildt, P. H., Allard, F., & Baron, E. 1999, ApJ, 512, 377
Hough, J. H., Lucas, P. W., Bailey, J. A., et al. 2006, PASP, 118, 1302
Husser, T.-O., Wende-von Berg, S., Dreizler, S., et al. 2013, A&A, 553, A6
Kemp, J. C., Henson, G. D., Barbour, M. S., Kraus, D. J., & Collins, II, G. W. 1983, ApJ, 273, L85
Koch, D. G., Borucki, W. J., Basri, G., et al. 2010, ApJ, 713, L79
Kostogryz, N. M., & Berdyugina, S. V. 2015, A&A, 575, A89
Kostogryz, N. M., Yakobchuk, T. M., Morozhenko, O. V., & Vid'Machenko, A. P. 2011, MNRAS, 415, 695
Kostogryz, N. M., Yakobchuk, T. M., & Berdyugina, S. V. 2015, ApJ, 806, 97
Kostogryz, N. M., Milic, I., Berdyugina, S. V., & Hauschildt, P. H. 2016, A&A, 586, A87
Lillo-Box, J., Barrado, D., Santos, N. C., et al. 2015, A&A, 577, A105
Lucas, P. W., Hough, J. H., Bailey, J. A., et al. 2009, MNRAS, 393, 229
Mayor, M., & Queloz, D. 1995, Nature, 378, 355
Piirola, V., Berdyugin, A., & Berdyugina, S. 2014, in Ground-based and Airborne Instrumentation for Astronomy V, Proc. SPIE, 9147, 91478
Rauer, H., Catala, C., Aerts, C., et al. 2014, Exp. Astron., 38, 249
Ricker, G. R. 2015, in AAS/Division for Extreme Solar Systems Abstracts, 3, 503.01
Wiktorowicz, S. J., & Laughlin, G. P. 2014, ApJ, 795, 12
Wiktorowicz, S. J., & Matthews, K. 2008, PASP, 120, 1282
Wiktorowicz, S. J., Nofi, L. A., Jontof-Hutter, D., et al. 2015, ApJ, 813, 48